Electrolytic Co-deposition of Zn-ZnO and Zn-ZnO-$CaCO_3$ Composite Substrates on Low-Carbon Steel

R. N. Nnaji[1], M. A. Bodude[2], D. E. Esezobor[3].

[1, 2, 3] Department of Metallurgical & Materials Engineering, University of Lagos, Lagos, Nigeria.

ABSTRACT: Conventionally employed zinc-rich paints and coatings for marine corrosion protection of steel still comprise environmentally unfriendly compounds such as zinc phosphate. This paper is focused on developing eco-friendly zinc ternary composite coatings of Zn-ZnO-$CaCO_3$ utilizing $CaCO_3$ additives derived from tympanotonus fuscatus (periwinkle) shell and calcareous eggshell respectively on low-carbon steel using electrodeposition technique. This is aimed at improving not only the surface corrosion resistance of steel structures in marine environment but also the sustainability of raw materials and minimal environmental pollution. Corrosion studies of uncoated and coated steel samples in simulated marine environment were done using linear polarization technique. Results obtained suggested that $CaCO_3$ (i.e., calcareous eggshell) additive in the composite coating significantly improved the corrosion performance of the substrate. Steel coated with calcareous eggshell additive displayed superior corrosion performance having highest polarization resistance, R_p (156090 Ω), lowest corrosion rate, *CR* (0.01 mm/year) and highest coating efficiency, C_{eff} (97%) as against those of uncoated, zinc oxide, and tympanotonus fuscatus shell additives after 30 minutes deposition time. Scanning Electron Microscopy (SEM) and Energy Dispersive X-Ray Spectroscopy (EDS) results of selected developed coatings indicated presence of a homogeneous surface morphology and a significant amount of calcium in the calcareous eggshell coating.

KEYWORDS: Coatings, electrodeposition, marine, steel, surface corrosion, zinc oxide.

[Received Aug. 17, 2022; Revised Oct. 4, 2022; Accepted Nov 6, 2022] Print ISSN: 0189-9546 | Online ISSN: 2437-2110

I. INTRODUCTION

Low-carbon steel is a versatile engineering material extensively employed across several industries such as oil and gas, and construction industries for structural applications (Larché and Dézerville, 2011). This is largely due to its ease of fabrication (weldability) and ease of recycling. However, low oxidation resistance leading to increased corrosion rate, especially in seawater and coastal marine environments is the major drawback of this class of steel (Fayomi, 2018; Garcia *et al*., 2014; Erten *et al*., 2015). Some economic implications of corrosion in industries such as the shipbuilding and maritime industries include: decrease in useful lifetime of steel-built ships and offshore steel installations; material losses (metal wastage – damaged ship hull); productivity and process operation losses (arising from delays); and reduction in overall system efficiency (Han *et al*., 2016; Norouzi and Afrasiabi-Garekani, 2014).

Marine environment conditions such as salinity, water temperature, and dissolved oxygen significantly influence the functionality of a corrosion protection coating and the surface corrosion mechanism of steel (Fayomi and Popoola, 2015; Momber *et al*., 2015). Constant immersion in seawater containing highly reactive chloride ions (Cl-) challenges the functionality of a corrosion protection coating and influences the corrosion rate of the steel surface. The corrosion rate defines the corrosion efficiency of the protective coating; and consequently, life span of the steel structure (Guedes-Soares *et al.*, 2011). Akinyele *et al*., (2021) investigated the influence of chloride on corrosion of steel embedded as reinforcement in concrete beams in marine environment. The mechanical properties of the steel observably reduced as a result of chloride (Cl-) attack.

Calcite, a polymorph mineral of the crystalline $CaCO_3$ is mainly utilized by the construction industry as marble or limestone in the production of cement and concrete (Janiszewska *et al*., 2018). Dahiru *et al*., (2018) studied the mechanical properties of concrete produced using periwinkle shell as coarse aggregate and suggested that partial replacement of the normal concrete aggregate was possible and effective for up to 25% addition. However, the corrosion resistance and stability of the periwinkle shell additive to marine environment conditions was not evaluated.

Zinc-rich paints on steel surfaces in marine environment provide barrier protection from air and moisture but do not provide sacrificial protection for the steel in an event of paint damage by mechanical impact and/or abrasion. The conventionally employed zinc-rich paints and marine coatings contain some environment unfriendly compounds such as

*Corresponding author: ruthnkirukannaji@gmail.com

doi: http://dx.doi.org/10.4314/njtd.v18i4.1314

zinc phosphate that are hazardous to both marine life and human health (Song *et al*., 2017; Popoola *et al*., 2013). Previous studies suggested the need for green solutions to corrosion control and inhibition of steel surfaces in chloride/acid service environments (Okewale and Adebayo, 2020).

The focus of this present study effort is to utilize affordable, sustainable, and locally available waste raw materials of tympanotonus fuscatus (t. fuscatus) shell and calcareous eggshell in the development of biocompatible and eco-friendly composite coatings on low-carbon steel using electrolytic co-deposition technique for improved surface corrosion resistance in marine simulated environment.

II. THEORETICAL ANALYSIS

The electrochemistry of the deposition process involves two major electrochemical reactions: anodic and cathodic reactions. Anodic reaction (oxidation/dissolution of zinc metal to ions) takes place at the zinc anode surface under the mildly acidic electrolyte condition as given in Eqn. 1:

$Zn\ (s) \rightarrow Zn^{2+}\ (aq) + 2e^{-}$ (oxidation/dissolution of zinc) (1)

The cathodic reaction (reduction/deposition of zinc ions as zinc atoms) simultaneously occurring on the steel surface is given in Eqn. 2:

$Zn^{2+}\ (aq) + 2e^{-} \rightarrow Zn\ (s)$ (reduction/deposition of zinc) (2)

Eqn. (2) is the electro-deposition/reduction of zinc ions in the electrolyte to zinc atoms on the steel surface, where -0.762 V is the reduction potential of zinc in neutral/acidic electrolyte. Therefore, the overall cell potential (redox potential) can be calculated by using Eqn. 3;

$$E^{0}_{cell} = E^{0}_{red} - E^{0}_{oxid} \quad (3)$$

Eqn. (3) translates to E^{0}_{cell} = [-0.762 - (-0.762)] V = 0 V. Hence, assuming no intermediate phase formations at the zinc anode; the net outcome is the reduction of zinc metal ions (dissolved ions) in the solution to Zn metal deposits (atoms) on the steel surface (cathode) with the application of an external amperage and minimal voltage (Shin *et al.*, 2020). However, other positive metal ions in the solution also get reduced at the cathode as a result of the current flow direction; hence, the zinc composite electrodeposition is possible. It is important to note that the electrodeposition process uses a cathodic protection approach; where the connection of the cathode (the low-carbon steel specimen) to the negative end of the direct current (DC) power supply puts the entire specimen surface into cathodic condition by maintaining a constant negative electrical charge on it. Consequently, the dissolution of iron in the solution as positive ions (Fe^{2+}) is inhibited (Carlile, 2008; Alias and Mohamad, 2015).

III. EXPERIMENTAL PROCEDURE

A. *Substrate Preparation*

Chemical composition and optical microstructure analyses of the as-received low-carbon steel were carried out at Midwal Engineering and Testing Laboratories, Lekki, Lagos, Nigeria. SpectroMAXx LMF06 Spectrometer (Spark Analyzer Pro MAXx Version 1.02.0001 software); manufacturer – AMETEK, Germany; Serial Number: 15007384) was used for the composition analysis; while, Metallurgical Microscope (500X capacity; serial no: AE2000MET; manufacturer: Metic Incorporation Limited) with a Biovis Material plus VA4.59 and Motic 2.0 software attached was used for optical microstructure analysis.

Low-carbon steel of dimensions 50 mm × 30 mm × 2 mm was used as the cathode in the present study; while two 99.9% pure zinc plates of dimensions 90 mm × 20 mm × 10 mm were used as the anodes. Each sample surface was ground using 220, 280, 360, 400, and 600-grit sizes of silicon carbide paper in succession to remove all surface oxides. Surface polishing of the samples was done using 3 μm diamond suspension followed by 1 μm diamond suspension on 3 μm and 1 μm Struers polishing cloths respectively. The samples were then washed under running water and dried using hot air. Prior to the electrodeposition process, cleaning and activation of the steel samples' surfaces were done using 0.01 M of sodium carbonate and 10% HCl acid solution at room temperature for approximately 10 seconds respectively (Ranganatha *et al*., 2012; Khodair *et al*., 2018). This was done to remove any possible dirt, oil, oxides, or residue contaminants left on the samples from the grinding and polishing processes. Surface activation of the zinc anodes was also done by dipping in the 10% HCl solution for a few seconds. The cleaning and activation of the experimental samples and zinc anodes was immediately followed by rinsing in deionized water.

B. *Processing of $CaCO_3$ Powder from Tympanotonus fuscatus Shell and Calcareous Eggshell Wastes*

Tympanotonus fuscatus shells obtained from Mushin market in Lagos State were roughly crushed, and washed several times using hot water and sun-dried for 36 hours over a six-day period (6 hours a day). Calcareous eggshell wastes from a domestic source were soaked in hot water for 20 minutes thrice in a row to facilitate removal of the inner membrane, followed by repeated washing using hot water. The eggshells were sun-dried for a total of 24 hours over a four day period (6 hours a day) to ensure complete dryness. Both shell wastes were pulverized and each of the powders was sieved to BSS/ASTM 400 mesh size. Figures 1 (a) and (b) show images of both as-received shell wastes. XRD characterization of each of the shell powders was carried out to identify the phases present.

(a)

(b)

Figure 1: Images of As-received (a) Tympanotonus fuscatus Shells, and (b) Calcareous Eggshells

C. Electrolytic Co-Deposition of Zn-ZnO-$CaCO_3$ Composite Coatings

The electrolytic co-deposition of Zn-ZnO, Zn-ZnO-$CaCO_3$ ($CaCO_3$ from t. fuscatus shell), and Zn-ZnO-$CaCO_3$ ($CaCO_3$ from calcareous eggshell) composite coatings on steel was performed respectively in a single cell containing two (2) zinc anodes and a single steel cathode (1) each time; all immersed in the solution at the same time as shown in the annotated picture of the set up in Figure 2.

The mildly acidic zinc sulphate solution was continuously stirred under moderate heating to improve the kinetics of the dissolved ions and dispersed particles. This also helped to prevent agglomeration of particles in the suspension. Table 1 shows the details of the bath additives and constituents for the three electrolytic deposition phases on low-carbon steel. The electrodeposition process conditions of voltage (1.4 V), temperature (45 °C), stirring rate (250 rpm), and pH (4.5) were kept constant at varied deposition time (15, 20, 25, and 30 minutes).

D. Electrochemical Corrosion Tests

Electrochemical corrosion analysis was carried out in simulated ocean water environment using 3.5% NaCl solution in a glass beaker containing 50 ml of the electrolyte each time. AUTOLAB Potentiostat Galvanostat (PGSTAT 101) - PC controlled with NOVA 2.1.2 software attached was used for the corrosion analyses and data recording. The analysis was done using uses a three-electrode setup: a silver/silver chloride (Ag/AgCl) reference electrode), a graphite counter electrode, and a working electrode (the test piece). Linear sweep voltammetry (LSV) was used to measure the potential delivered through the 3-electrode system from the Potentiostat Galvanostat. The voltage was scanned from -1.5 to 1.5 V at a scan rate of 0.01 V/s at room temperature for approximately 428 seconds for each individual run. The samples were stabilized at open-circuit for 2 minutes before the actual polarization measurements were recorded each time. To ensure reproducibility, the analysis was repeated three different times for samples of matching compositions.

E. Scanning Electron Microscopy

Surface microstructure characteristics and composition changes of selected corrosion-tested specimens were examined using ASPEX 3020 Scanning Electron Microscope (SEM) domiciled in the Materials Testing Laboratory at the Department of Materials Science and Engineering, Kwara State University (KWASU), Malete. The composition changes were detected using Energy Dispersive X-ray Spectroscopy (EDS). Results of the SEM and EDS analyses are detailed in the next section.

IV. RESULTS AND DISCUSSION

A. Chemical Composition and Optical Microstructure of Low-carbon Steel Used

Low-carbon steel with chemical composition (wt. %) shown in Table 2 and optical microstructure shown in Figure 3 was used as the cathode in this study.

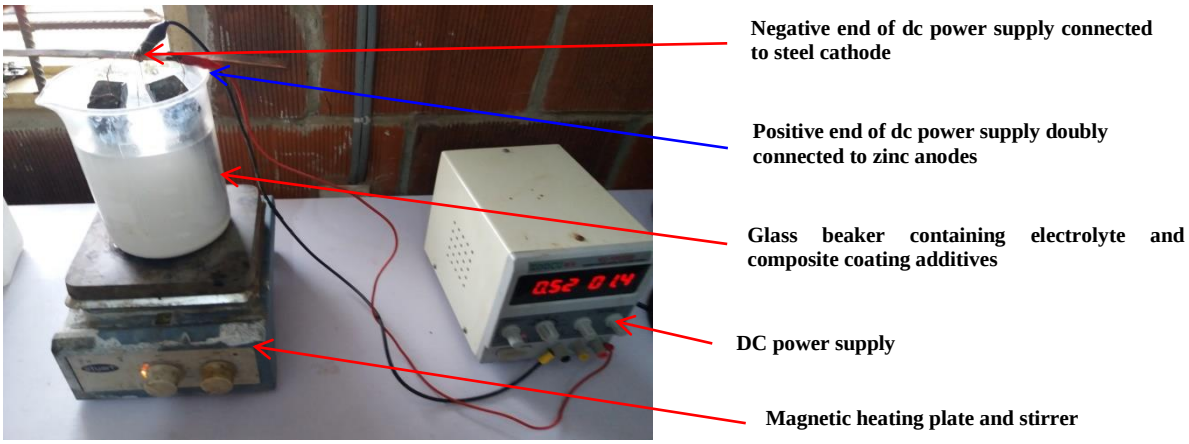

Figure 2: Electrolytic co-deposition set up of Zn-ZnO-$CaCO_3$ coatings on low-carbon steel

Table 1 Zinc sulphate bath composition for Zn-ZnO-$CaCO_3$ electrodeposition on low-carbon steel

Additive/ Constituent	$ZnSO_4{\cdot}7H_2O$	K_2SO_4	H_3BO_3	Thiourea	Glycine	ZnO	$CaCO_3$ (t. fuscatus shell powder)	$CaCO_3$ (calcareous eggshell powder)
Mass concentration (g/l)	100	30	20	10	10	15	20	20

Table 2 Chemical composition (wt. %) of as-received low-carbon steel

Element	C	Si	Mn	P	S	Cr	Al	Fe
Wt. %	0.041	0.004	0.092	0.017	0.002	0.029	0.010	99.8

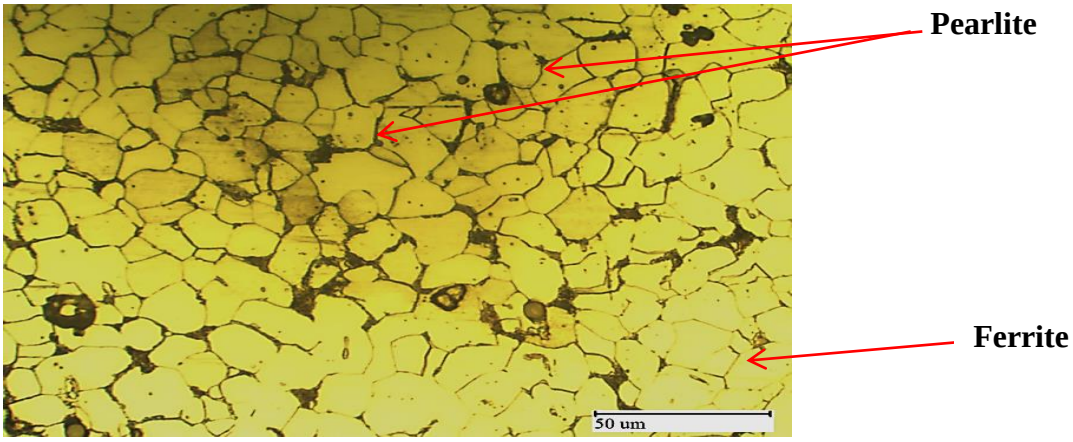

Figure 3: Optical micrograph (500*X*) showing the ferrite-pearlite microstructure of as-received low-carbon steel

B. X-Ray Diffraction Analyses of T. Fuscatus Shell and Calcareous Eggshell Powders

The analyses revealed the phase and chemical composition of the t. fuscatus shell powder shown in Figure 4 as 81% aragonite ($Ca_{4.00}\ C_{4.00}\ O_{12.00}$), 10% calcite ($Ca_{5.62}\ Mg_{0.38}\ C_{6.00}O_{18.00}$), and 9% quartz ($Si_{3.00}\ O_{6.00}$) and the calcareous eggshell powder shown in Figure 5 as 78% calcite ($Ca_{6.00}\ C_{6.00}\ O_{18.00}$) and 22% aragonite ($Ca_{4.00}\ C_{4.00}O_{12.00}$). The crystallographic systems of the phases as-identified were hexagonal for calcite, orthorhombic for aragonite, and hexagonal for quartz accordingly.

C. Weight of Composite Coatings Deposited on Low-Carbon Steel

The samples weight before and after the coating depositions were measured and recorded to ascertain the weight of coating deposited for a given electrodeposition time. A plot of coating weight deposited with time is shown in Figures 6, 7, and 8 for the three electrodeposition phases - Zn-ZnO, Zn-ZnO-$CaCO_3$ (t. fuscatus shell), and Zn-ZnO-$CaCO_3$ (calcareous eggshell) respectively.

The Zn-ZnO curve displayed a linear progression of weight of coatings electrodeposited on steel substrates with

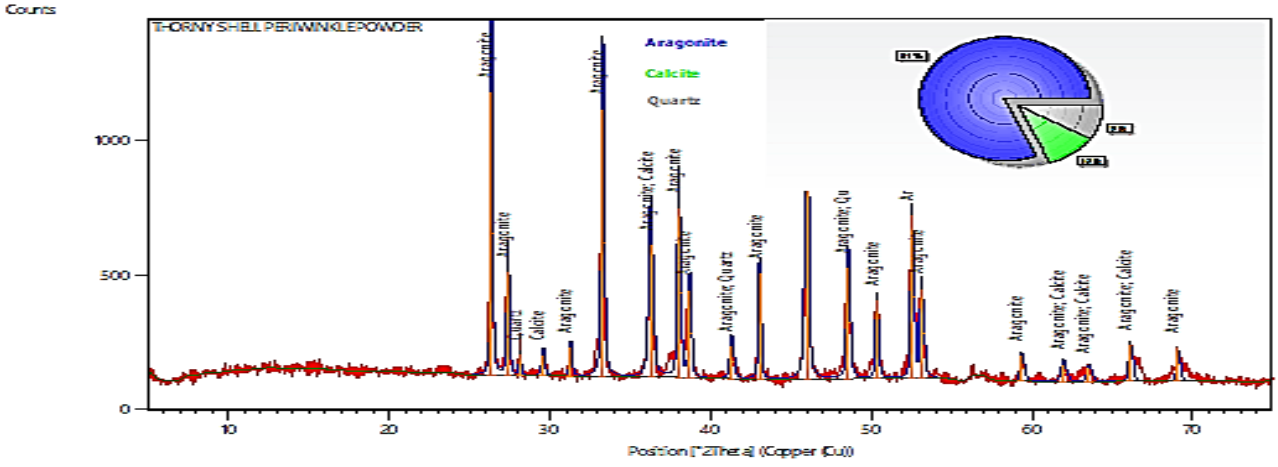

Figure 4: XRD Pattern of T. Fuscatus Shell Powder

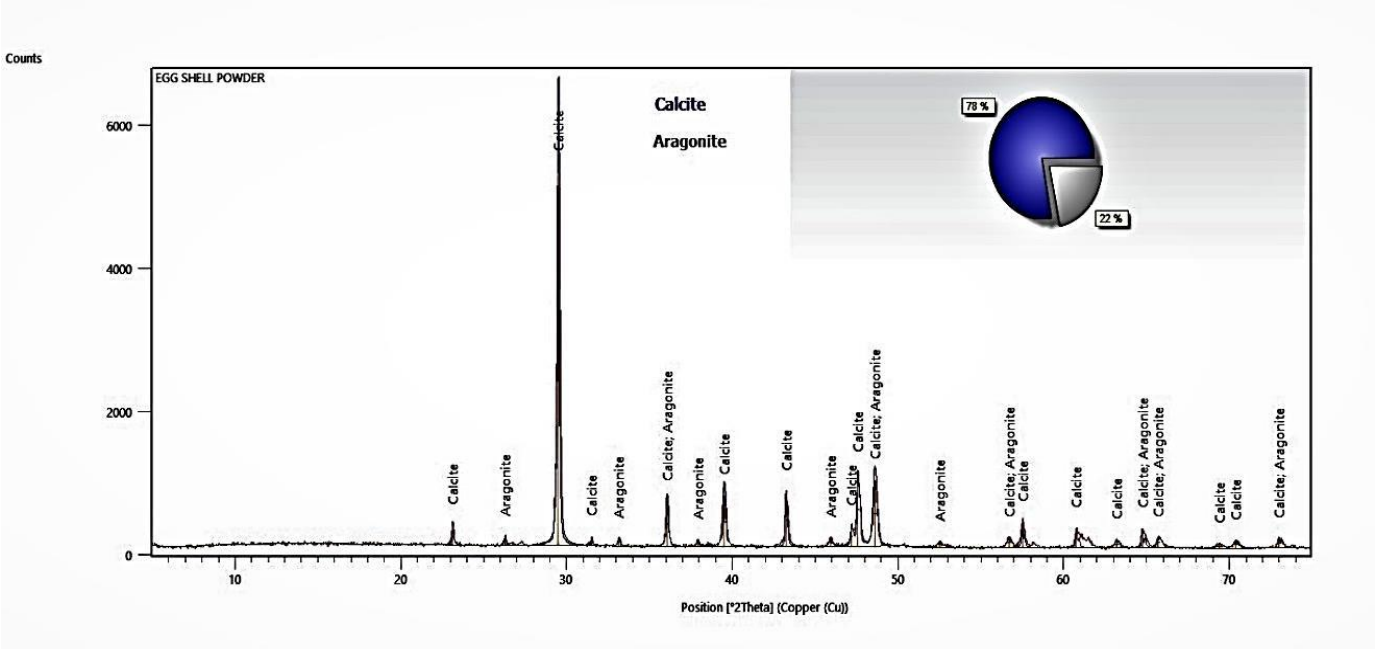

Figure 5: XRD Pattern of Calcareous Eggshell Powder

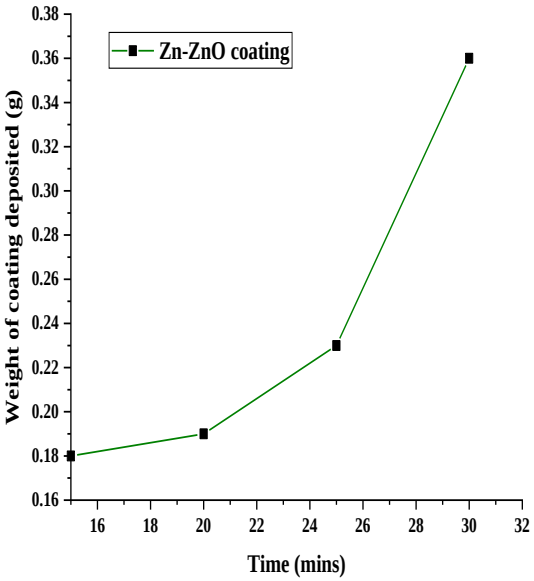

Figure 6: Plot showing weight of coating deposited vs. time for Zn-ZnO electrodeposition on low-carbon steel substrates

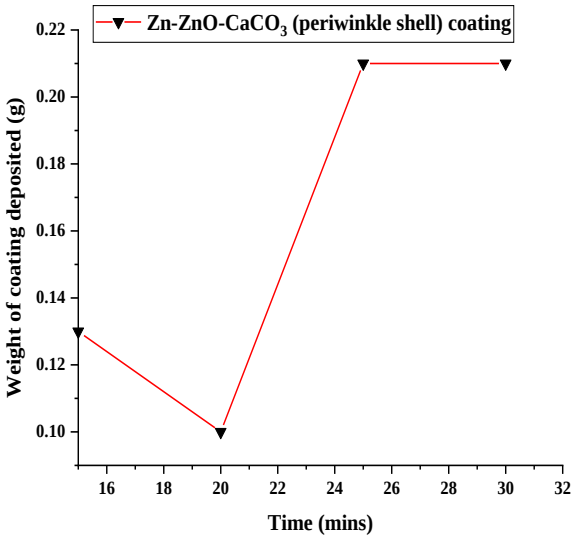

Figure 7: Plot showing weight of coating deposited vs. time for Zn-ZnO-$CaCO_3$ (t. fuscatus shell) electrodeposition on low-carbon steel

time as shown in Figure 6, while the Zn-ZnO-$CaCO_3$ (t. fuscatus shell) coating curve pattern shown in Figure 7 is non-uniform. The Zn-ZnO-$CaCO_3$ (calcareous eggshell) composite coating plot shown in Figure 8 had the highest weight (0.52 g) of coating deposited after 30 minutes duration; displaying a quasi-linear trend in coating weight deposited with time. The weight of coating deposited decreased steadily from 15 to 25 minutes, and then a sharp increase after 30 minutes deposition time. Suggestively, the increase in time allowed the stabilization of the bath temperature, which positively impacted the weight of coating deposited.

D. Electrochemical Corrosion Performance of Uncoated and Coated Low-Carbon Steel

Polarization curves of the potential (*e*) versus log current density (log *j*) from the linear sweep voltammetry data for the uncoated, Zn-ZnO, Zn-ZnO-$CaCO_3$ (t. fuscatus), and Zn-ZnO-$CaCO_3$ (calcareous eggshell) composite coated steel specimens are shown in Figures 9, 10, and 11 respectively. LPS (linear polarised sample) is an identification tag for the experimental specimens, where LPS 1 - 4, LPS 5 - 8, and LPS 9 -12 in the figures' legends as well as in Table 3 in this section represent the results obtained for samples electro coated for 15, 20, 25, and 30 minutes for each of the three different deposition phases

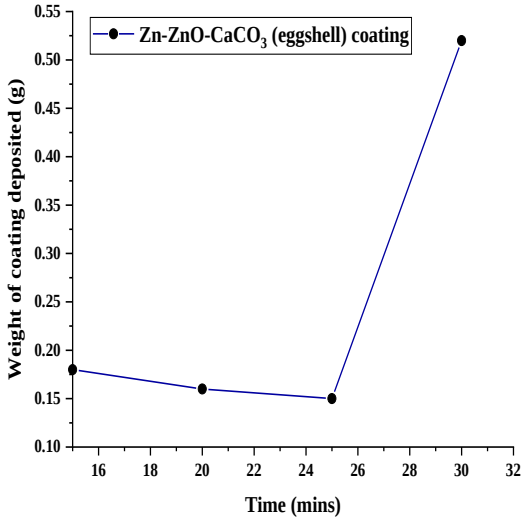

Figure 8: Plot showing weight of coating deposited vs. time for Zn-ZnO-$CaCO_3$ (calcareous eggshell) electrodeposition on low-carbon steel

(Zn-ZnO, Zn-ZnO-$CaCO_3$ - t. fuscatus shell, and Zn-ZnO-$CaCO_3$ - calcareous eggshell) respectively.

As-observed, data points of LPS 5, 6, and 7 in Figure 10 coincided with LPS 8; hence the polarization curves seem fewer than the legends shown on the right. However, evidence of the curves can be seen from the electrode potential, *e* (V) end pointing to E_{corr} on the Y-axis.

The potentiodynamic polarization resistance (***Rp***), corrosion rate, ***CR*** (mm/year), and estimated coating efficiency (C_{eff}) of the coated samples recorded are outlined in Table 3. The corrosion protection ability of the composite coatings was estimated as the coating efficiency (C_{eff}) (Akande *et al.*, 2018; Khodair *et al.*, 2018] relative to the corrosion rate using the relationship in Eqn. 4.

$$\text{Coating efficiency } (C_{eff}) = \left(\frac{CR_0 - CR_n}{CR_0}\right) x\ 100 \quad (4)$$

Where, CR_0 = corrosion rate of uncoated steel specimen

CR_n = corrosion rate of zinc composite coated steel specimen.

As-observed, the uncoated substrate had the least polarization resistance of 21620 Ω and the highest corrosion

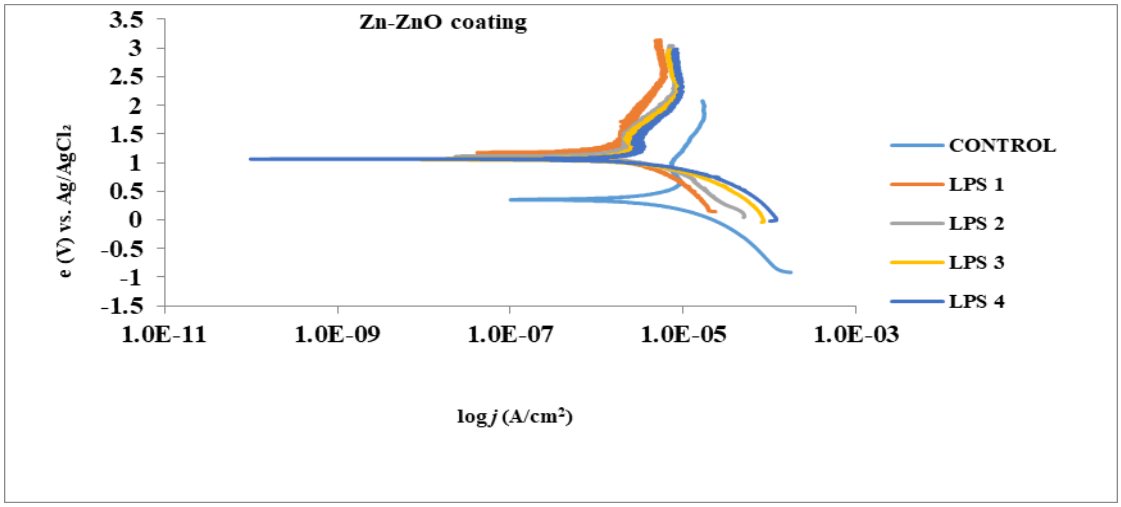

Figure 9: Polarization Curve of Electrode Potential versus Log Current Density of Uncoated and Zn-ZnO Coated Substrates

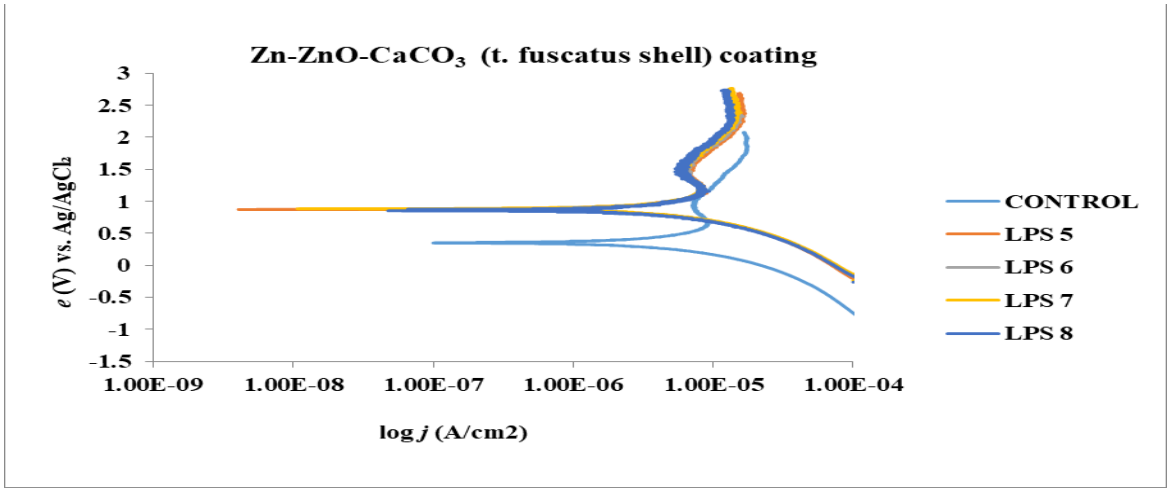

Figure 10: Polarization Curve of Electrode Potential versus Log Current Density of Uncoated and Zn-ZnO-$CaCO_3$ (t. fuscatus shell) Coated Substrates

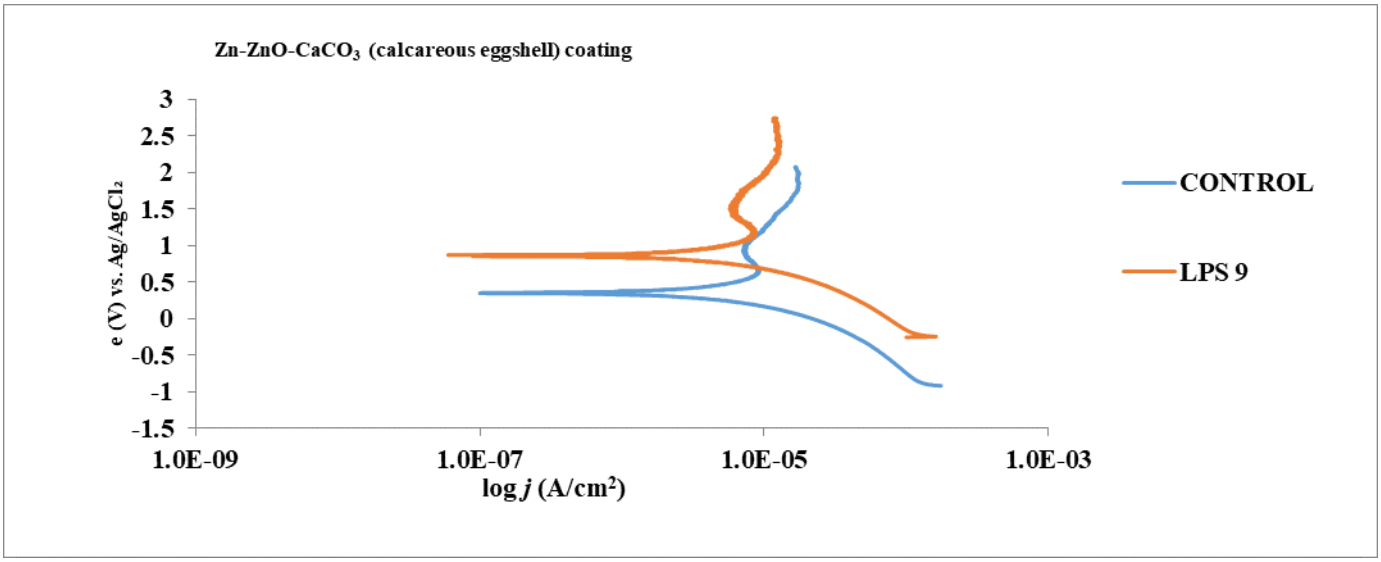

Figure 11: Polarization Curve of Electrode Potential versus Log Current Density of Uncoated and Zn-ZnO-$CaCO_3$ (calcareous eggshell) Coated Substrates.

Table 3 Electrochemical corrosion performance of zinc composite coated low-carbon steel

Sample tag	Coating Additive	*Rp* (Ω)	*CR* (mm/yr)	C_{eff} (%)
CONTROL	N/A	21620	0.36	N/A
LPS 1	Zn-ZnO	74706	0.09	75
LPS 2		45705	0.17	53
LPS 3		35233	0.16	56
LPS 4		37956	0.05	89
LPS 5	Zn-ZnO-$CaCO_3$	22178	0.22	39
LPS 6	(t. fuscatus shell)	22861	0.28	22
LPS 7		22575	0.32	11
LPS 8		22132	0.24	33
LPS 9	Zn-ZnO-$CaCO_3$	22562	0.24	33
LPS 10	(calcareous eggshell)	132440	0.01	97
LPS 11		139350	0.07	81
LPS 12		156090	0.01	97

***N/A** (Not applicable)

rate of 0.36 mm/yr. As shown in Table 3, the polarization resistances and corrosion rates of the Zn-ZnO-$CaCO_3$ (t. fuscatus shell) coatings were relatively poor. Hence, the estimated coating efficiencies were correspondingly poor. However, the corrosion rates of all t. fuscatus shell coated steel samples were lower in comparison with the control (uncoated steel). This could be attributable to the significant presence of zinc in the coating as seen from the EDS composition analysis. The Zn-ZnO-$CaCO_3$ (calcareous eggshell) - 20 and 30 mins coated samples, displayed the best surface corrosion performance, having lowest corrosion rates of 0.01 mm/yr and coating efficiencies of 97% in each case.

E. SEM and EDS Results of Corrosion-Tested Coated Samples

The surface morphology of the polarized Zn-ZnO coated steel (25 minutes deposition time) showed presence of pores (indicated by the red arrows) in the SEM image shown in Figure 12 (a). The presence of pores in a surface coating will enhance easy penetration of moisture and electrolyte species to the underlying substrate. Consequently, the corrosion protection efficiency of the coating will be reduced. Therefore, the porosity of a surface coating is a significant property to be considered in evaluating its corrosion protection ability.

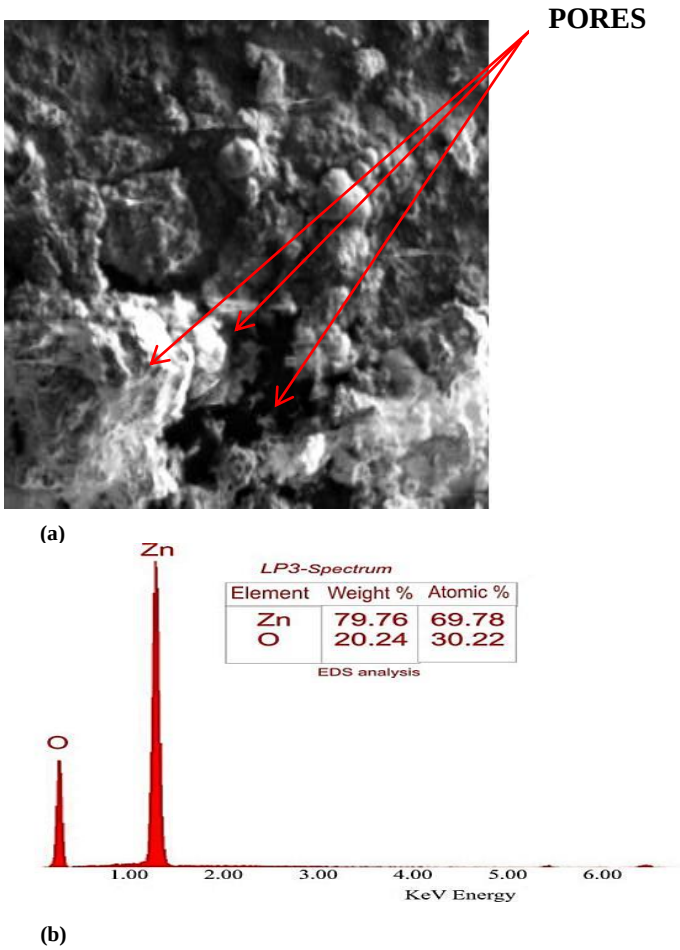

Figure 12: Surface (a) SEM Image (500*X*), and (b) EDS Spectrum of Polarized Steel Sample coated with Zn-ZnO (25 minutes deposition time)

The SEM image shown in Figure 13 (a) for Zn-ZnO-$CaCO_3$ (t. fuscatus shell) coated substrate (25 minutes

deposition time) presented a smooth surface morphology in comparison with the ZnO and calcareous eggshell additive coatings. However, it displayed the highest corrosion rate (0.32 mm/yr.) and least coating efficiency (11%) in comparison with the coated samples having ZnO and eggshell additives. Comparatively, the SEM surface morphology of Zn-ZnO-$CaCO_3$ (calcareous eggshell) substrate coated for 25 minutes shown in Figure 14 (a), as observed is more homogeneous. The EDS analyses for Zn-ZnO, Zn-ZnO-$CaCO_3$ (t. fuscatus), and Zn-ZnO-$CaCO_3$ (calcareous eggshell) coatings are shown in Figures 12 (b), 13 (b), and 14 (b) as charts with X-axis (Energy) in kilo-electron-volt (keV), and Y-axis (Intensity) in counts per second units respectively.

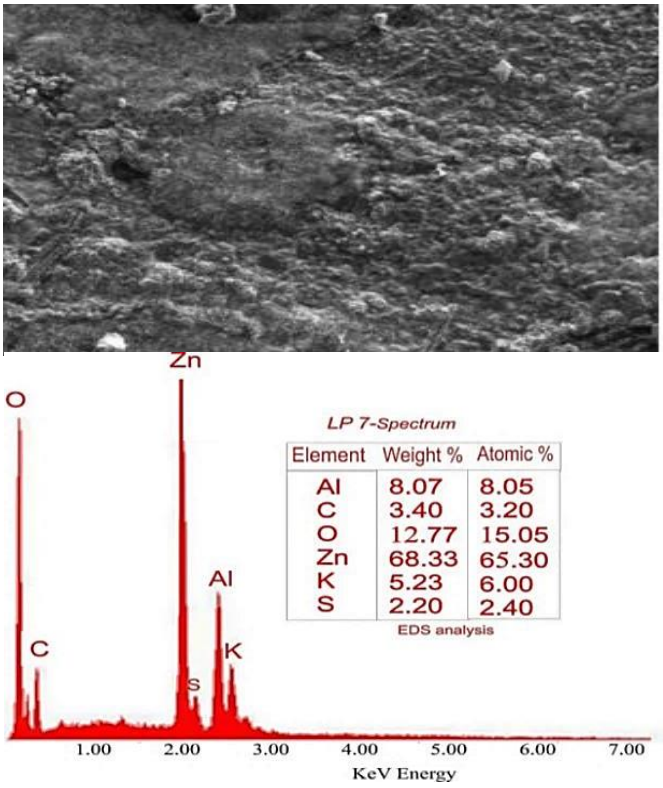

(b)

Figure 13: Surface (a) SEM Image (500*X*), and (b) EDS Spectrum of Polarized Steel Sample coated with Zn-ZnO-$CaCO_3$ (t. fuscatus shell) (25 minutes deposition time)

Aluminium (Al), potassium (K), and sulphur (S) detected in the Zn-ZnO-$CaCO_3$ (t. fuscatus) coating EDS result may have been environmental contaminations acquired during sample handling during or after electrodeposition or before the SEM analysis; as neither these elements nor compounds containing the elements were detected from the XRD analysis of the powder prior to the electrodeposition process. It has been reported that the presence of sulphur in zinc coatings led to formation of deleterious compounds with zinc, which promoted high surface corrosion rates in the substrate (Smith *et al.*, 2017). More so, the substrate will degrade faster if the corrosion products are formed at the substrate/coating interface rather than the coating/electrolyte boundary (Refait *et al.*, 2017).

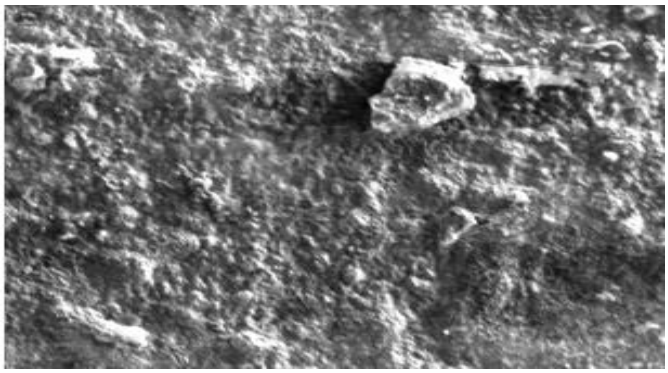

(a)

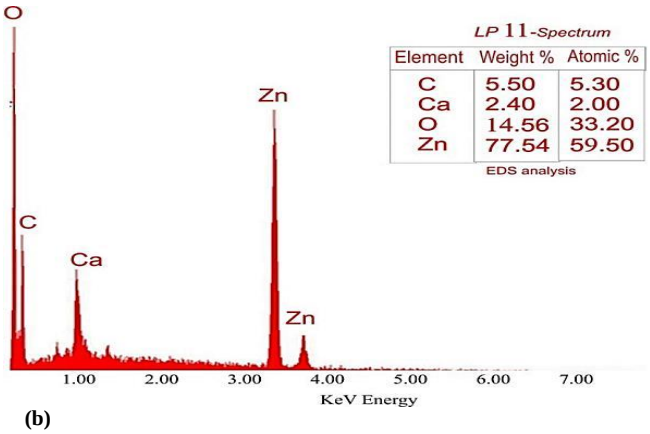

(b)

Figure 14: Surface (a) SEM Image (500*X*), and (b) EDS Chart of Polarized Steel Sample coated with Zn-ZnO-$CaCO_3$ (calcareous eggshell)

V. CONCLUSION

Zn-ZnO-$CaCO_3$ composite coatings, with $CaCO_3$ obtained from agro-wastes of t. fuscatus shell and calcareous eggshell were successfully developed on low-carbon steel substrates. The Zn-ZnO-$CaCO_3$ (t. fuscatus shell) coated samples generally, displayed the highest corrosion rates in the environment considered in comparison with the ZnO and eggshell additive coatings examined. The Zn-ZnO-$CaCO_3$ (t. fuscatus shell) plot exhibited an irregular pattern of weight of coating deposited with time; hence, it is suggested that other deposition process variables influenced this behaviour. The EDS analysis result of the Zn-ZnO-$CaCO_3$ (t. fuscatus shell) composite coating (25 minutes deposition time) also alludes to the above suggestion as no calcium was detected in the coating deposit. The coated samples of both Zn-ZnO and Zn-ZnO-$CaCO_3$ had lower corrosion rates in comparison with the uncoated sample. $CaCO_3$ (calcareous eggshell) additive in the coating improved the surface corrosion performance of the steel in simulated marine environment.

However, future studies will seek to investigate the structure, adhesion, microstructure, specifically the aspect of porosity, and the microbiologically influenced corrosion

resistance of the developed $CaCO_3$ composite coatings on mild steel to further validate stability in marine environment.

ACKNOWLEDGMENTS

Special thanks to Prof. O. S. I. Fayomi of the Department of Mechanical Engineering, Bells University of Technology, Otta, Ogun State, Nigeria, for providing laboratory facilities and scientific advice to support this study. The authors are appreciative of the continued technical assistance of the Management and staff of MIDWAL ENGINEERING (Metallurgical Engineers and Testing Laboratory), Lekki, Lagos, Nigeria.

AUTHOR CONTRIBUTIONS

R. N. Nnaji: Conceptualization, Methodology, Investigation, Resources, Writing – original draft preparation. **M. A. Bodude** and **D. E. Esezobor:** Conceptualization, Supervision. **R. N. Nnaji** and **D. E. Esezobor:** Writing – reviewing & editing.

REFERENCES

Akande, I. G.; O. O. Oluwole and O. S. I. Fayomi. (2018). Optimizing the defensive characteristics of mild steel via the electrodeposition of $ZnSi_3N_4$ reinforcing particles. *Defence Technology*, 15(4): 526-532.

Akinyele, J. O.; U. T. Igba; F. M. Alayaki and S. I. Kuye. (2021). Modelling the deformation of steel-bars in reinforced concrete beams submerged in lagoon. *Nigerian Journal of Technological Development*, 18(3): 219-228.

Alias, N. and A. A. Mohamad. (2015). Morphology study of electrodeposited zinc from zinc sulfate solutions as anode for zinc-air and zinc-carbon batteries. Journal of King Saud University - *Engineering Sciences*, 27(1), 43–48.

Carlile, A. (2008). Cathodic protection monitoring: Techniques for Corrosion Monitoring. Woodhead Publishing Series in Metals and Surface Engineering, 448–475.

Dahiru, D.; U. S. Yusuf and N. J. Paul. (2018). Characteristics of concrete produced with periwinkle and palm kernel shells as aggregates. FUTY, Journal of the Environment, 12(1): 42-61.

Erten, Ü.; H. İ. Ünal; S. Zor and Ş. H. Atapek. (2015). Structural and electrochemical characterization of $Zn–TiO_2$ and $Zn–WO_3$ nanocomposite coatings electrodeposited on St 37 steel. *Journal of Applied Electrochemistry*, *45*(9): 991-1003.

Fayomi, O. S. I. (2018). Effect of functional composite coating developed via sulphate and chloride process parameter on the UNS G10150 steel for structural and wear mitigation in defence application. Elsevier, *Defence technology*, *14*(3): 196-203.

Fayomi, O.S.I. and Popoola, A.P.I. (2015). Development of smart oxidation and corrosion resistance of multi-doped complex hybrid coatings on mild steel. Elsevier, *Journal of Alloys and Compounds*, 637, 382-392.

Garcia, J. R.; D. C. B. D. Lago and L. F. D. Senna. (2014). Electrodeposition of cobalt rich Zn-Co alloy coatings from citrate bath. *Materials Research*, *17*(4): 947-957.

Guedes-Soares, C.; Y. Garbatov and A. Zayed. (2011). Effect of environmental factors on steel plate corrosion under marine immersion conditions. Corrosion Engineering, Science and Technology, 46(4): 524–541.

Han, H. S.; K. H. Lee and S. H. Park. (2016). Parametric study to identify the cause of high torsional vibration of the propulsion shaft in the ship. Elsevier, *Engineering Failure Analysis*, *59*, 334-346.

Janiszewska, K.; M. Mazur; M. Machalski and J. Stolarski. (2018). From pristine aragonite to blocky calcite: Exceptional preservation and diagenesis of cephalopod nacre in porous Cretaceous limestones. PLos ONE, 13(12): e0208598

Khodair, Z. T.; A. A. Khadom and H. A. Jasim. (2018). Corrosion protection of mild steel in different aqueous media via epoxy/nanomaterial coating: preparation, characterization and mathematical views. *Journal of Materials Research and Technology*, *8*(1), 424-435.

Larché, N. and Dézerville, P. (2011). Review of material selection and corrosion in seawater reverse osmosis desalination plants. Taylor & Francis, *Desalination and Water Treatment*, 31(1-3): 121-133.

Momber, A. W.; P. Plagemann and V. Stenzel. (2015). Performance and integrity of protective coating systems for offshore wind power structures after three years under offshore site conditions. Elsevier, *Renewable energy*, *74*, 606-617.

Norouzi, M. and A. Afrasiabi-Garekani. (2014). Corrosion protection by zirconia-based thin films deposited by a sol–gel spin-coating method. Ceramics International, 40(2): 2857–2861.

Okewale, A. O. and A. T. Adebayo. (2020). Thermodynamic and optimization studies of castor leaf extract as corrosion inhibitor on stainless steel (301). *Nigerian Journal of Technological Development*, 17(3), 229-238.

Popoola, L. T.; A. S. Grema; G. K. Latinwo, B. Gutti and A. S. Balogun. (2013). Corrosion problems during oil and gas production and its mitigation. Springer, *International Journal of Industrial Chemistry*, 4(1): 1-15.

Ranganatha, S.; T. V. Venkatesha; K. Vathsala and M. K. P. Kumar. (2012). Electrochemical studies on Zn/nano-CeO_2 electrodeposited composite coatings. Elsevier, *Surface and Coatings Technology*, 208, 64–72.

Refait, P.; A.-M. Grolleau; M. Jeannin, E. François and R. Sabot. (2017). Corrosion of mild steel at the seawater/sediments interface: Mechanisms and kinetics. *Corrosion Science*, 130, 76–84.

Shin, J.; J. Lee; Y. Park and J. W. Choi. (2020). Aqueous Zinc Ion Batteries: Focus on Zinc Metal Anodes. Royal Society of Chemistry, *Chemical Science*, 11, 2028-2044.

Smith, J. G.; X. Zhang and P. K. Jain. (2017). Galvanic reactions at the single-nanoparticle level: tuning between mechanistic extremes. Royal Society of Chemistry, *Journal of Materials Chemistry A*, 5(23), 11940–11948.

Song, Y.; G. Jiang; Y. Chen, P. Zhao and Y. Tian. (2017). Effects of chloride ions on corrosion of ductile iron and carbon steel in soil environments. Springer Nature, *Scientific Reports*, 7(1): 1-13.